Arctic Science

OPEN ACCESS | Article

Mapping tundra ecosystem plant functional type cover, height, and aboveground biomass in Alaska and northwest Canada using unmanned aerial vehicles

Kathleen M. Orndahl[a], **Libby P.W. Ehlers**[b], **Jim D. Herriges**[c], **Rachel E. Pernick**[d], **Mark Hebblewhite**[b], **and Scott J. Goetz**[a]

[a]School of Informatics, Computing and Cyber Systems, Northern Arizona University, 1295 Knoles Dr., Flagstaff, AZ 86011, USA; [b]W.A. Franke College of Forestry and Conservation, University of Montana, 32 Campus Dr., Missoula, MT 59812, USA; [c]Bureau of Land Management, 222 University Ave., Fairbanks, AK 99709, USA; [d]Independent Researcher, St. George, UT 84770, USA

Corresponding author: **Kathleen M. Orndahl** (email: kmo265@nau.edu)

Abstract

Arctic vegetation communities are rapidly changing with climate warming, which impacts wildlife, carbon cycling, and climate feedbacks. Accurately monitoring vegetation change is thus crucial, but scale mismatches between field and satellite-based monitoring cause challenges. Remote sensing from unmanned aerial vehicles (UAVs) has emerged as a bridge between field data and satellite-based mapping. We assessed the viability of using high-resolution UAV imagery and UAV-derived Structure from Motion to predict cover, height, and aboveground biomass (henceforth biomass) of Arctic plant functional types (PFTs) across a range of vegetation community types. We classified imagery by PFT, estimated cover and height, and modeled biomass from UAV-derived volume estimates. Predicted values were compared to field estimates to assess results. Cover was estimated with a root-mean-square error (RMSE) of 6.29%–14.2%, and height was estimated with an RMSE of 3.29–10.5 cm depending on the PFT. Total aboveground biomass was predicted with an RMSE of 220.5 g m^{-2}, and per-PFT RMSE ranged from 17.14 to 164.3 g m^{-2}. Deciduous and evergreen shrub biomass was predicted most accurately, followed by lichen, graminoid, and forb biomass. Our results demonstrate the effectiveness of using UAVs to map PFT biomass, which provides a link towards improved mapping of PFTs across large areas using earth observation satellite imagery.

Key words: Arctic tundra, vegetation mapping, drones, UAV, structure from motion

Résumé

Les communautés végétales de l'Arctique changent rapidement avec le réchauffement climatique, ce qui influence la faune, le cycle du carbone et les rétroactions climatiques. Il est donc crucial de surveiller avec précision les changements de la végétation, mais les disparités d'échelle entre la surveillance sur le terrain et la surveillance par satellite posent des défis. La télédétection à partir de véhicules aériens sans pilote (UAV) est apparue comme un pont entre les données de terrain et la cartographie par satellite. Les auteurs évaluent la viabilité de l'utilisation de l'imagerie haute résolution par des UAV et de la structure acquise à partir du mouvement (SfM – *Structure from Motion*) d'UAV pour prédire la couverture, la hauteur et la biomasse hors-sol (ci-après biomasse) de types fonctionnels de plantes (PFT — *Plant functional types*) de l'Arctique dans une gamme de types de communautés végétales. Ils ont classé l'imagerie par PFT, estimé la couverture et la hauteur, et modélisé la biomasse à partir des estimations de volume obtenues par UAV. Les valeurs prédites ont été comparées aux estimations sur le terrain pour évaluer les résultats. La couverture a été estimée avec écart moyen quadratique (EMQ) de 6,29-14,2 % et la hauteur a été estimée avec un EMQ de 3,29-10,5 cm, selon le PFT. La biomasse hors-sol totale a été prédite avec un EQM de 220,5 g m-2, et l'EQM par PFT variait de 17,14 à 164,3 g m-2. La biomasse des arbustes à feuilles caduques et à feuilles persistantes a été prédite avec le plus de précision, suivie par la biomasse des lichens, des graminoïdes et des herbes non graminéennes. Ces résultats démontrent l'efficacité de l'utilisation d'UAV pour cartographier la biomasse de PFT, ce qui établit un lien vers cartographie améliorée des PFT sur de grandes superficies grâce à l'imagerie satellitaire d'observation de la terre. [Traduit par la Rédaction]

Mots-clés : toundra arctique, cartographie de la végétation, drones, UAV, structure acquise à partir d'un mouvement

Introduction

Arctic regions are experiencing some of the fastest rates of climate warming in the world (Richter-Menge et al. 2019), leading to significant changes in vegetation composition and structure (Berner et al. 2020; Bjorkman et al. 2018; Myers-Smith et al. 2019; Pearson et al. 2013). Increasing vegetation productivity and deciduous shrub expansion are among the most prevalent of these changes. Shifts in vegetation communities are expected to have cascading effects: i.e., impacting wildlife forage and habitat (Mallory and Boyce 2018; Post et al. 2009), carbon cycling and storage (Abbott et al. 2016; Lafleur and Humphreys 2018; Mack et al. 2004), permafrost dynamics (Abbott et al. 2016; Lawrence and Swenson 2011; Nauta et al. 2015; Schuur et al. 2015), and potentially contributing to further warming (Chapin et al. 2005; Loranty and Goetz 2012). As such, accurate and precise monitoring of Arctic vegetation is crucial.

Because vegetation species do not respond uniformly to shifts in climate, and because changes in species composition do not have uniform downstream effects, it is useful to monitor and map vegetation across ecologically meaningful groups. For example, vegetation community types describe assemblages of plant species that co-occur, typically due to similar environmental requirements (Lortie et al. 2004; Viereck et al. 1992). These groupings provide insight into the landscape context within which individual plants exist and define dominant plant species. However, because these groupings are categorical, large variations in species composition can occur within vegetation community types (Macander et al. 2017). In contrast, plant functional types (PFTs) group plants based on their function within ecosystems, determined by morphological, phylogenetic, and (or) phenological traits (Chapin et al. 1996; Thomas et al. 2018). PFTs can be monitored and mapped individually, providing precise quantitative measures of plant cover across landscapes. Monitoring and mapping vegetation structure add an important dimension to our understanding of vegetation change. In particular, vegetation biomass is a high-priority trait for monitoring because it is closely tied with ecological function and determines carbon storage (Houghton et al. 2009). Therefore, deriving fine grain information on vegetation biomass, partitioned by PFT, may help Arctic ecologists understand the consequences of climate change on carbon and nutrient cycling, patterns of shrub expansion and corresponding declines in other PFTs (e.g., lichens), disturbance regimes, and wildlife/vegetation interactions (Bernes et al. 2015; Bjorkman et al. 2018; Chapin 2003; Myers-Smith et al. 2020; Olofsson and Post 2018; Schmitz et al. 2018).

Field measurements of vegetation cover, height, and aboveground biomass (henceforth biomass) are widely used to accurately monitor vegetation changes over time (Bjorkman et al. 2020; Myers-Smith et al. 2019). However, such measurements are time and resource intensive and therefore limited in spatial scope and coverage (Bjorkman et al. 2020). In contrast, remote sensing from satellites can provide regional or even global-scale monitoring of vegetation communities. However, vegetation monitoring with satellites is typically conducted at moderate to coarse spatial resolution (10 m–1 km), which makes mapping challenging across heterogenous landscapes. Higher resolution satellite data exist but are generally not freely available (Langford et al. 2016; Räsänen et al. 2018). The scale discrepancy between field data and readily available satellite imagery makes it difficult to link plot-level observations to regional- or global-scale satellite observations (Cunliffe et al. 2020; Siewert and Olofsson 2020).

Remote sensing from unmanned aerial vehicles (UAVs) provides high-resolution imagery (sub-centimeter to several meters) at landscape scales and has emerged as a natural "bridge" between highly detailed but spatially sparse field measurements and coarse resolution but spatially extensive satellite remote sensing (Poley and McDermid 2020; Riihimäki et al. 2019; Siewert and Olofsson 2020). UAVs show promise for measuring structural traits, such as vegetation height and biomass (Cunliffe et al. 2021; Poley and McDermid 2020), especially in tundra ecosystems (Alonzo et al. 2020; Cunliffe et al. 2021; Fraser et al. 2016). Capable UAV platforms are now reasonably priced ($1600 + USD) and can be outfitted with a variety of sensors: high-resolution RGB, multispectral, hyperspectral, thermal, and even lidar (light detection and ranging).

Structure from Motion (SfM) is emerging as a cost-effective method for capturing vegetation structure (Alonzo et al. 2020; Cunliffe et al. 2021). SfM works by identifying matching features in overlapping images and triangulating these features to create three-dimensional reconstructions. Most software for processing UAV imagery (e.g., Pix4 D, Agisoft) include SfM in their processing workflow, which allows users to create detailed point clouds. In fact, SfM point clouds are typically denser than lidar point clouds (Poley and McDermid 2020). The main drawback of SfM is its inability to penetrate overlying vegetation. However, discrete return lidar can also fail to penetrate the canopy where vegetation is short in stature and canopy gaps are small relative to the instrument's footprint (Greaves et al. 2015).

Tundra vegetation communities are ideal candidates for SfM because vegetation is often sparse, and tree/shrub canopies rarely obscure the ground completely. However, the understory of lichens and mosses can make it challenging to define the "ground" surface in tundra ecosystems (Greaves et al. 2016). Deciduous shrub biomass has been mapped in the Arctic using satellite imagery (Berner et al. 2018; Chen et al. 2012), terrestrial and airborne lidar (Alonzo et al. 2020; Greaves et al. 2015, 2016), airborne SfM (Alonzo et al. 2020), and UAV-based SfM (Alonzo et al. 2020; Cunliffe et al. 2021). Although to our knowledge biomass has not been estimated with SfM for non-shrub Arctic PFTs specifically, SfM-derived canopy height was a strong predictor of graminoid and forb biomass across a global study of non-forest ecosystems (Cunliffe et al. 2021). Furthermore, SfM results in dryland ecosystems resolved grass tussock volume to within 1 cm^3 (Cunliffe et al. 2016), providing a reasonable and promising

analog to cottongrass (*Eriophorum* spp.) tussock tundra, which is widespread in the Low Arctic (Walker et al. 2005).

Here, we explore the feasibility of employing UAVs for mapping biomass of several PFTs (deciduous shrubs, evergreen shrubs, graminoids, lichens, forbs) in tundra ecosystems and at the tundra/taiga ecotone. We focused on one primary research question: (1) How accurately can biomass be modeled across PFTs using UAVs? We recognize, however, that landscape context could influence how well particular PFTs are modeled. For example, graminoid biomass might be better modeled in tussock tundra, where sedges form distinct clumps, versus non-tussock tundra where graminoids are dispersed across the landscape, even if the same amount of graminoid biomass is present. For this reason, we include a secondary research question: (2) Does the accuracy with which PFT biomass is modeled differ depending on which vegetation community type the PFT is situated in?

Methods

Study area

We visited 44 sites during the summer of either 2018 or 2019 to collect field data and UAV imagery (Table S1). Study sites were located across interior Alaska and northwest Canada and were selected to represent the variety of vegetation community types present on the landscape, focusing on arctic and alpine tundra (Fig. 1, Table S1). Our study area encompassed the Alaska and Yukon North Slope, several mountain ranges (Brooks Range, Richardson Mountains, Ogilvie Mountains) and interior Alaska–Yukon lowlands. The arctic and subarctic sites in our study are characterized by low precipitation, short, cool summers and long, cold winters with mean annual temperature ranging from −13 °C to −5 °C, and annual precipitation ranging from 150 to 330 mm. Growing seasons are short, ranging from 126 to 177 days (Scenarios Network for Alaska and Arctic Planning 2009). We aimed to visit sites close to peak summer greenness, but this was not always possible due to site access constraints.

Data collection

Site setup

We collected data at ten 0.25 m^2 quadrats per site, spaced 10 m apart along a 100 m transect (Fig. 1C). The transect tape was run parallel to topographic contour lines to minimize variation in elevation across the site. The tape was staked to avoid movement in the wind, and care was taken to not trample vegetation within quadrats. Wood stakes/PVC pipe were placed at the lower left corner of each quadrat so that the quadrats could be located in the UAV imagery (Fig. 1B).

Quadrat photos

Ground-based, nadir-oriented photos were taken of each quadrat with a handheld digital camera. Under sunny conditions, a tarp was used to shade the quadrats to ensure consistent lighting and minimize shadows.

Cover data

At each quadrat, we recorded ocular estimates of top cover (cover sums to 100%; Wilson 2011) by species. To reduce observer bias in cover estimates, all observers were trained in ocular estimation. We discussed estimates among observers to "calibrate" estimates, provided reference material showing different arrangements of known cover percentages, and used quadrats with edge markings every 10 cm so quadrats could be easily subdivided visually (Morrison 2016). Each quadrat was assigned a vegetation community type designation based on *The Alaska vegetation classification* (Viereck et al. 1992) level III classes (Table S2). Classes were assigned using ground-based quadrat photos and ocular cover estimates for reference, following the key provided by *The Alaska vegetation classification* (Viereck et al. 1992). These vegetation community type designations expand on those listed in Table S1 because sites were sometimes heterogenous with more than one vegetation community type present.

Height data

At each quadrat, we recorded three height measurements per species to allow for estimation of average height across the quadrat. Measurements were taken using a ruler and lowering until firm resistance was met at the duff/soil layer. Height was recorded as the location where the ruler was intersected by the tallest plant part (stem, leaf, inflorescence). When tussocks were present, we took two separate measurements: (1) from the ground to the top of the tussock and (2) from the top of the tussock to the top of the live sedge blades/stems.

Biomass harvest

Plant aboveground biomass was harvested at five 0.25 m^2 quadrats per site (Fig. 1C). Within each quadrat, we clipped biomass to ground level, where ground was considered the rock, bare soil, duff, or moss surface. While harvesting, the quadrat sides were treated as strict boundaries—vegetation segments that extended outside the quadrat boundary were excluded from harvest, even if they were rooted in the plot, and vegetation segments that branched into the quadrat were included, even if they were rooted outside the plot. Harvested biomass was sorted into PFTs: shrubs, graminoids, forbs, and lichens (crustose lichens and lichens growing on rock were excluded) for 2018 harvests; shrubs were further partitioned into deciduous shrubs and evergreen shrubs in 2019. During data entry, 2018 shrub biomass data were partitioned into deciduous shrubs and evergreen shrubs when it was possible to do so (e.g., only evergreen shrub cover was recorded at the quadrat). When these data could not be confidently partitioned, they were excluded from data processing and analysis. Harvested biomass was stored in paper bags, dried in a ventilated drying oven at 65 °C for 48 h (to a constant weight), and weighed to the nearest 0.001 g. Mosses were excluded from harvest due to time constraints at sites. At our remote sites, access was dictated by aircraft and time-limited. Although we recognize the importance of

Fig. 1. (A) Site locations (red dots) where UAV imagery and vegetation plot data were collected. (B) Inset showing quadrat layout and dimensions. (C) Layout of sites—black squares represent quadrat locations with green dots denoting quadrats at which biomass was harvested, red lines represent the lawnmower flight path of the UAV, crossed rectangles represent the location of ground control points (not to scale). Map sources (A): Esri, GEBCO, NOAA, National Geographic, DeLorme, HERE, Geonames.org, and other contributors, (B) and (C): Created in ArcGIS Pro software.

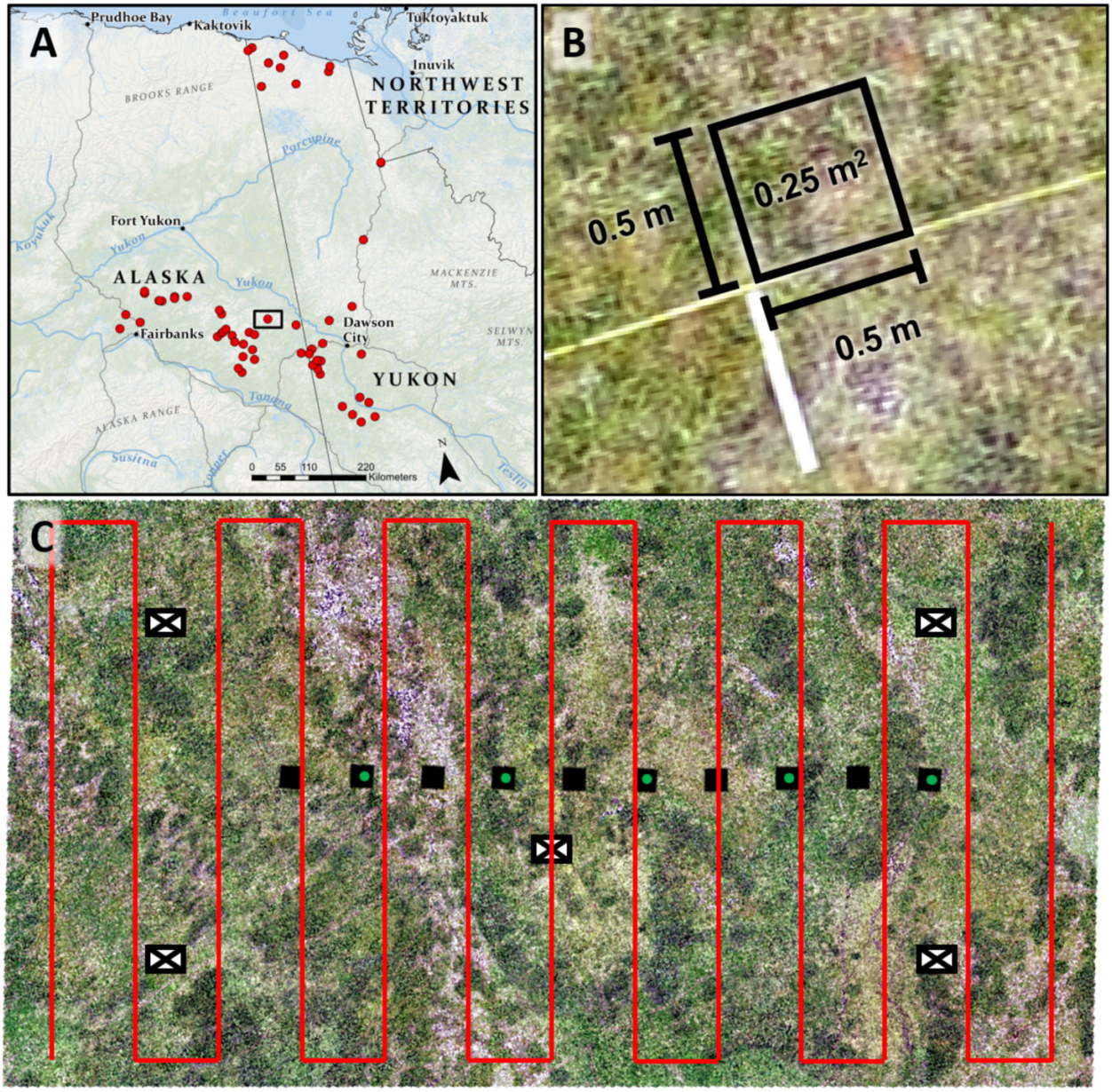

mosses in boreal and Arctic ecosystems (Turetsky et al. 2012), we excluded them here because they were the most time consuming to harvest, and we did not feel we could confidently distinguish them from the ground surface in our modeling.

Unmanned aerial vehicle flights

We used a DJI Phantom 4 Pro quadcopter UAV (P4P) for imagery collection. The P4P was equipped with the stock RGB camera, a MicaSense RedEdge-M multispectral camera with red, green, blue, red edge, and near-infrared bands, and a downwelling light sensor linked to the MicaSense and mounted atop the UAV. At each site, we conducted autonomous flights in a "lawnmower" pattern (Fig. 1C). Flights were centered around the 100 m quadrat transect and averaged 0.02 km^2 in area (0.005–0.177 km^2). We flew the UAV at 30 m above ground level (agl) (Cunliffe et al. 2016; Fraser et al. 2016; Poley and McDermid 2020). Test flights confirmed that 30 m agl produced consistent image-processing results. Ground sampling distances were approximately 0.75 cm for RGB imagery and approximately 2 cm for multispectral imagery. Front and side image overlap were set at 85%, flight

speed was capped at 2 m/s, and white balance was set to sunny or cloudy, depending on weather conditions. The RGB camera captured images in JPG format, and the MicaSense captured images in TIF format. We oriented the RGB camera and MicaSense sensor to nadir for all flights. In 2018, we gathered additional imagery with the RGB camera pointed 30° off-nadir for one pass around the outside of the site. In 2019, we flew an additional flight across the entire site with the RGB camera pointed at 30° off-nadir and flight lines perpendicular to the nadir flight. Off-nadir imagery provided additional viewing angles and improved reconstruction of the ground surface (Cunliffe et al. 2016). We aimed to fly close to solar noon and under consistent lighting conditions (Assmann et al. 2019; Poley and McDermid 2020), but this was not always possible due to site access constraints. Before and after each flight, we used the MicaSense sensor to take an image of a MicaSense calibrated reflectance panel, ensuring no shadows were cast upon the panel. To georeference our imagery, we placed five ground control points across each site in a quincunx pattern (Fig. 1C) and recorded their X, Y, and Z locations with a Trimble GeoXH handheld unit with satellite-based augmentation systems (SBAS) enabled to increase accuracy (X, Y accuracies 10–50 cm, Z accuracies 10–150 cm with SBAS).

Unmanned aerial vehicle imagery processing

Preprocessing

Initial UAV image processing was conducted using Pix4mapper (Pix4D SA 2021) (Fig. 2A). We calibrated the multispectral imagery using reflectance values from the downwelling light sensor and from the calibrated reflectance panel photos. We then marked and added geolocation information for ground control points. Finally, we processed the imagery to produce site orthophoto mosaics and densified point clouds. Point clouds from the RGB imagery were used in all future analyses, as they were denser than those produced from multispectral imagery. The multispectral mosaics were manually co-registered to the RGB mosaics in ArcMap Pro (Environmental Systems Research Institute Inc.. 2021). Additional preprocessing details are provided in Supplementary Text 1.

Plant functional type classification

For each site, we generated a database of calibration/validation samples by manually delineating polygons of target PFTs (deciduous shrubs, evergreen shrubs, forbs, graminoids, lichens) and non-target classes (bryophytes, non-vegetated, trees) on top of RGB imagery in ArcGIS Pro (Environmental Systems Research Institute Inc.. 2021). We used the ground-based quadrat photographs as a reference to identify PFTs in the imagery but did not create calibration/validation data within quadrat boundaries. Each site was modeled separately using pixel-based scikit-learn (Pedregosa et al. 2011) random forest classifier models in Python 3.7 (Van Rossum and Drake 2009), with spectral predictors derived from UAV imagery (Table S3). Additional information about these predictors is given in Supplementary Text 2.

First, we performed nested cross-validation (5 inner splits, 10 outer splits) on a subset of eight sites to determine optimal hyperparameters (Table S4). These sites were chosen to represent the variety of vegetation community types found across all 44 sites. For hyperparameter tuning, we focused on the number of variables available for splitting at each node (max_features), the size of each bootstrap sample (max_samples), and the minimum number of observations in a terminal node (min_samples_leaf) as previous research indicates these are often the most influential parameters (Huang and Boutros 2016; Probst et al. 2019). Using the optimal hyperparameters, we performed a 10-fold cross-validation for each site to determine the overall and per-PFT accuracy (Table S5). Cross-validation models were run with 500 trees, used an 80%/20% calibration/validation split, were stratified by PFT, and were grouped by calibration/validation polygon to minimize spatial autocorrelation. Because our classification groups were imbalanced, we oversampled calibration sets using the Synthetic Minority Oversampling Technique (SMOTE) from the imblearn Python package (Lemaître et al. 2017; Sun et al. 2009). Finally, we used the optimal hyperparameters to build models on the full predictor set and produced PFT classifications for each site (Figs. 2B, 3B). For the final models, we assessed predictor importance with Shapely values using the SHAP (SHapley Additive exPlanations) Python package (Lundberg et al. 2020). This method reduces bias from correlated and (or) differently scaled predictors (Nandlall and Millard 2020).

Evaluating PFT classification error

To understand how PFT impacted the accuracy of predicted cover we aggregated both our ground-based ocular estimates of cover and our pixel-based classifications at the quadrat, PFT level. Species-specific ocular estimates of cover were aggregated into PFTs, producing % cover estimates for each PFT within each quadrat. Classifications were aggregated at the quadrat level, producing % cover estimates for each PFT within each quadrat. Ground-based estimates were taken as "truth" and used to validate estimates from the classification.

The quadrat-level cover data were right skewed and contained a large proportion of zeros. This can make it difficult to identify an appropriate modeling approach, as many modeling approaches of interest do not work well in the presence of zeros (Fletcher et al. 2005). To overcome this, we filtered the data into two sets and used a different modeling approach for each set (Fletcher et al. 2005).

The first data set (henceforth presence/absence data) included all the available quadrat-level data. Using these data, we created two binary response variables denoting whether a commission error was made for each PFT (*commission*), and whether an omission error was made for each PFT (*omission*). If the quadrat-level cover from the classification was ≥1% and the quadrat-level ground-based cover estimate was <1%, *commission* was assigned a value of 1, otherwise it was assigned a value of 0. Conversely, if the classification cover was <1% and the ground-based cover was ≥ 1%, *omission* was assigned

Fig. 2. Workflow for processing UAV imagery: (A) pre-processing using Pix4 D software to create site-wide mosaics and densified point clouds (B) classifying site-wide mosaics using random forest classifier, (C) creating canopy height models using lidR package in R, (D) modeling biomass using canopy height models and field biomass harvest data, and (E) partitioning biomass by plant functional type.

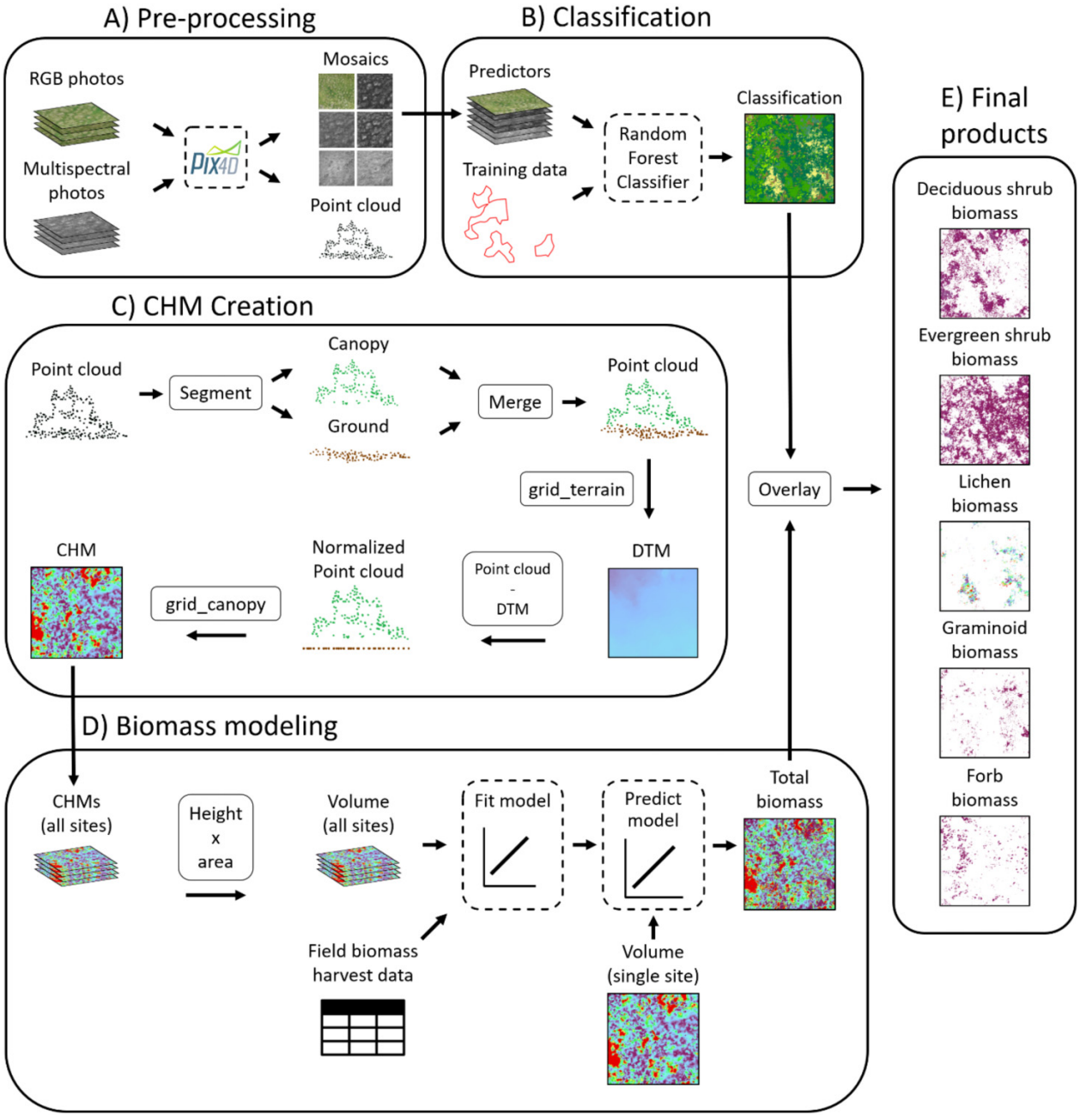

a value of 1, otherwise it was assigned a value of 0. We modeled commission and omission error proportion using logistic regression via the glm function in R v4.0.2 (R Core Team 2020) using the binomial family, and PFT as the sole predictor. We built two separate models, one for commission error proportion, and one for omission error proportion. We plotted the modeled commission and omission error proportions (converted to %) along with 95% confidence intervals and tested for differences in commission/omission proportions among PFTs using the Kruskal–Wallis test, followed by Dunn's tests with Bonferroni adjustments for multiple pairwise comparison. To test for potential pseudoreplication introduced by quadrats nested within sites, we used the intraclass correlation coefficient (ICC) from the ICC package (Wolak 2016) in R v4.0.2 (R Core Team 2020) to assess similarity in quadrat-level *commission* and *omission* values within sites. The ICC values were 0.05 and 0.04, respectively, indicating low correlation within sites and little evidence of pseudoreplication.

The second data set (henceforth presence-only data) included only quadrat-level observations where a PFT was accurately predicted as present in a quadrat. This data set ex-

Fig. 3. Example of UAV imagery products: (A) RGB imagery, (B) classification, (C) canopy height model, (D) biomass predictions, and (E) uncertainty estimates (95% confidence intervals). Created in ArcGIS Pro software.

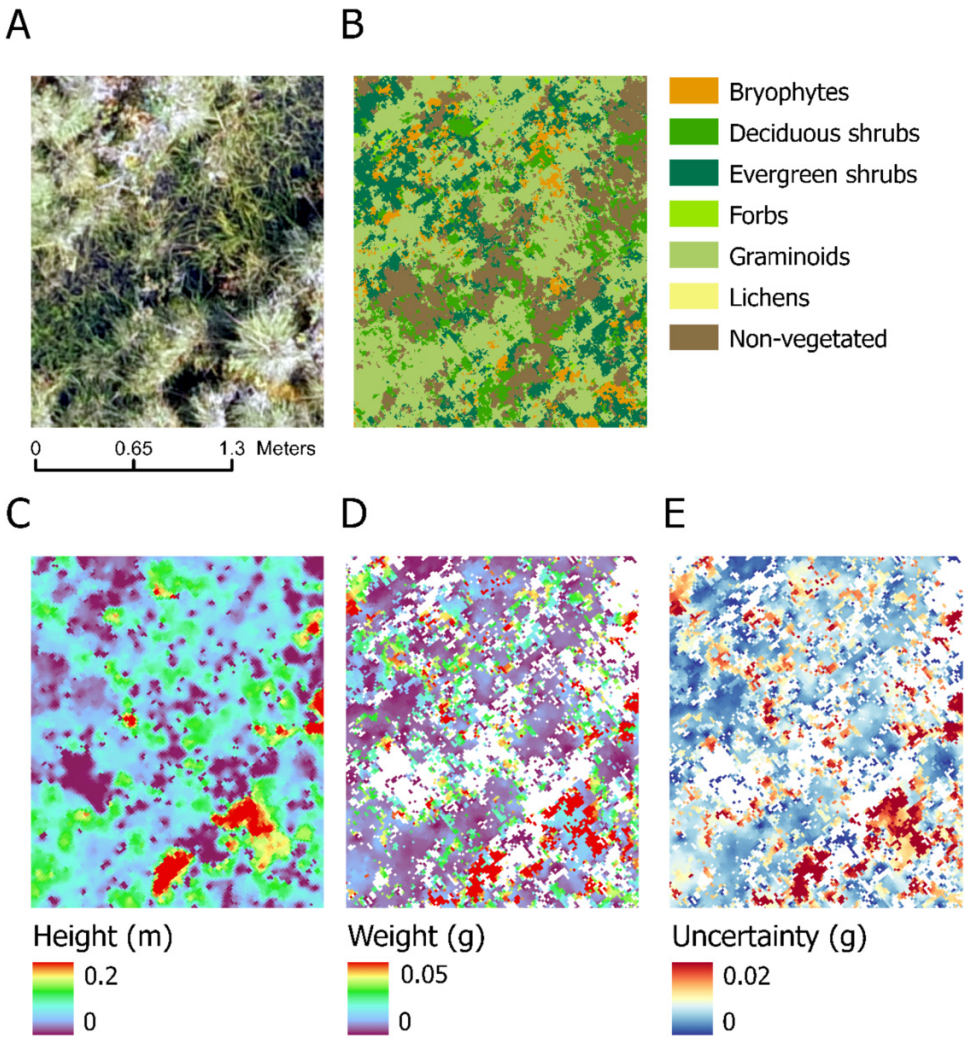

cluded a large number of instances where cover was correctly predicted as 0%. These instances confounded interpretation by deflating error for rarer PFTs. The presence-only data set was assessed using a continuous response variable representing the magnitude of prediction error. We used the relative % difference (RPD) in our analysis, defined as

$$\text{RPD} = 2\frac{|\text{cover}_{\text{actual}} - \text{cover}_{\text{predicted}}|}{\text{cover}_{\text{actual}} + \text{cover}_{\text{predicted}}} \times 100 \quad (1)$$

The relative % difference metric was useful because it penalized overpredictions and underpredictions equally.

To test for significant differences in distributions of relative % difference values we used the Kruskal–Wallis test, followed by Dunn's tests with Bonferroni adjustments for multiple pairwise comparison. We applied these tests to several groupings of the presence-only data set: (1) grouped by PFT only, (2) grouped by vegetation community type only, and (3) grouped by PFT and vegetation community type. We again tested for pseudoreplication using the ICC to assess similarity in quadrat-level relative % difference values within sites. The ICC value was 0.01, indicating low correlation within sites and little evidence of pseudoreplication.

Canopy height model generation for biomass estimation

Point cloud filtering

Point clouds were automatically filtered to exclude noise and outliers in Pix4Dmapper (Pix4D SA 2021). In addition, we manually inspected point clouds in CloudCompare 2.11.3 (CloudCompare 2021) and clipped out any visibly erroneous points.

Ground/canopy segmentation

To produce accurate digital terrain models (DTMs), we separated point clouds into "ground" and "canopy" points using a three-step process (Fig. 2C). First, we applied a focal maxi-

mum and focal minimum function to each point cloud. For each pass, the lowest/highest values in a 1–2 cm × 1–2 cm rolling window were retained creating a subset of ground and canopy points, respectively. Next, a nearest neighbor algorithm was applied to the ground and canopy subsets to filter out erroneous ground/canopy labels. For each point, this algorithm considered its 24 nearest neighbors and retained the lowest/highest point in this neighborhood. Finally, the resulting ground and canopy subsets were compared to the results from the PFT classification. Only ground points that fell within an area classified as non-vegetated or bryophytes were retained, and only canopy points that fell within an area classified as deciduous shrubs, evergreen shrubs, forbs, graminoids, lichens, or trees were retained. Filtering using the PFT classification allowed us to remove erroneous ground/canopy labels. For example, in a dense shrub thicket there might be no legitimate ground points. The lowest/highest Z and nearest neighbor steps would identify the lowest point and label it ground even though it is actually part of the shrub canopy, which would lead to errors when interpolating the ground surface. Since this point is in an area classified as deciduous shrub, it is instead discarded in the final filtering step.

Point cloud normalization

We created a DTM from the ground points using the grid_terrain function from the lidR package (Roussel et al. 2020; Roussel and Auty 2020) in R v4.0.2 (R Core Team 2020) with a k-nearest neighbors inverse distance weighting (knnidw) algorithm (Fig. 2C). This algorithm interpolates across the entire site, producing a seamless DTM. The DTM was then subtracted from the point cloud, producing a normalized point cloud. After normalization any points with height < 0 were discarded since these represented erroneous height values.

Canopy height model creation

Finally, we created canopy height models (CHMs) using the grid_canopy function from the lidR package and the normalized point cloud (Supplementary Text 3; Figs. 2C, 3C). The CHM resolution was the average distance between points before filtering, typically 1–2 cm. This resolution provided the best balance between minimizing empty cells and maximizing product resolution. We used a simple point to raster algorithm (p2r from the lidR package) to generate the CHM.

After CHM generation, height values less than zero were converted to zero and empty cells were filled using a 3 × 3 pixel focal mean. In areas where normalized point density was low, processing artifacts were present in the CHM. We converted these areas to empty cells using the method described in Supplementary Text 3. We then filled these data gaps by creating a random forest regressor for each site using scikit-learn (Pedregosa et al. 2011) in Python (Van Rossum and Drake 2009). The regressor predicted height within gaps using predictors derived from the UAV imagery listed in Table S3.

Canopy volume calculation

CHMs were converted to volume (cm^3) by multiplying each pixel value (height; cm) by pixel area (cm^2).

Aboveground biomass estimation

For each site, we overlaid the volume map and classification and summed pixels to determine the total volume per PFT in each quadrat. These quadrat-level volume observations were linked with biomass harvest data from the corresponding quadrat and PFT. We then used these observations to model PFT aboveground biomass using linear mixed-effect models fit using the lme4 package (Bates et al. 2014) in R (Fig. 2D) as follows:

$$\begin{aligned} \text{m} \;=\; & \text{lmer}\left(\text{biomass} \sim 0 + \text{volume} : \text{PFT}\right. \\ & + \left.\left(0 + \text{volume} : \text{PFT} \mid \text{site}\right), \text{data} = \text{data}\right) \end{aligned} \tag{2}$$

PFT was included as a fixed effect, site was included as a random effect, and intercepts were constrained to the origin because zero volume corresponds with zero biomass. Both the response and predictor variables were square root transformed to reduce heteroskedasticity and non-normality of the residuals. The biomass-volume model was then applied to each volume raster, producing per pixel biomass predictions (Fig. 3D; for more details, see Supplementary Text 4). We also calculated 95% confidence intervals for each biomass prediction (Bolker 2021) producing per pixel estimates of uncertainty (Fig. 3E; Supplementary Text 4).

The data used for building the biomass-volume models were filtered to ensure only the highest quality data influenced the model. For each PFT, the quadrat-level observations were arranged in descending order by cover error (|field observed cover—cover predicted by classification|) and the top 20% of observations (highest error) were excluded from modeling. This prevented the worst misclassifications from being carried forward in the analysis. We also excluded observations where volume was equal to zero, and biomass was greater than zero and vice versa as these represented verifiable errors in the volume prediction.

To understand how PFT and vegetation community type impacted biomass prediction accuracy, we tested for significant differences following the procedure described in the section *Evaluating PFT classification error*. For this analysis, we again excluded the 20% of quadrat-level observations with the highest cover error for each PFT. This was done to focus on prediction errors that were due to errors in the CHM and (or) uncertainty in the biomass-volume model and not errors in cover estimation. We used only the presence-only data set as factors influencing presence/absence were well captured by the analysis described in the section *Evaluating PFT classification error*.

Results

Plant functional type classification

The normalized difference vegetation index (NDVI) was the most important predictor for our classification (Table S3),

Fig. 4. Comparison of field observed % cover (*y*-axis) and predicted % cover from random forest modeling (*x*-axis). Each point represents a quadrat. The dashed line shows the one-to-one line. The solid black line shows the line of best fit.

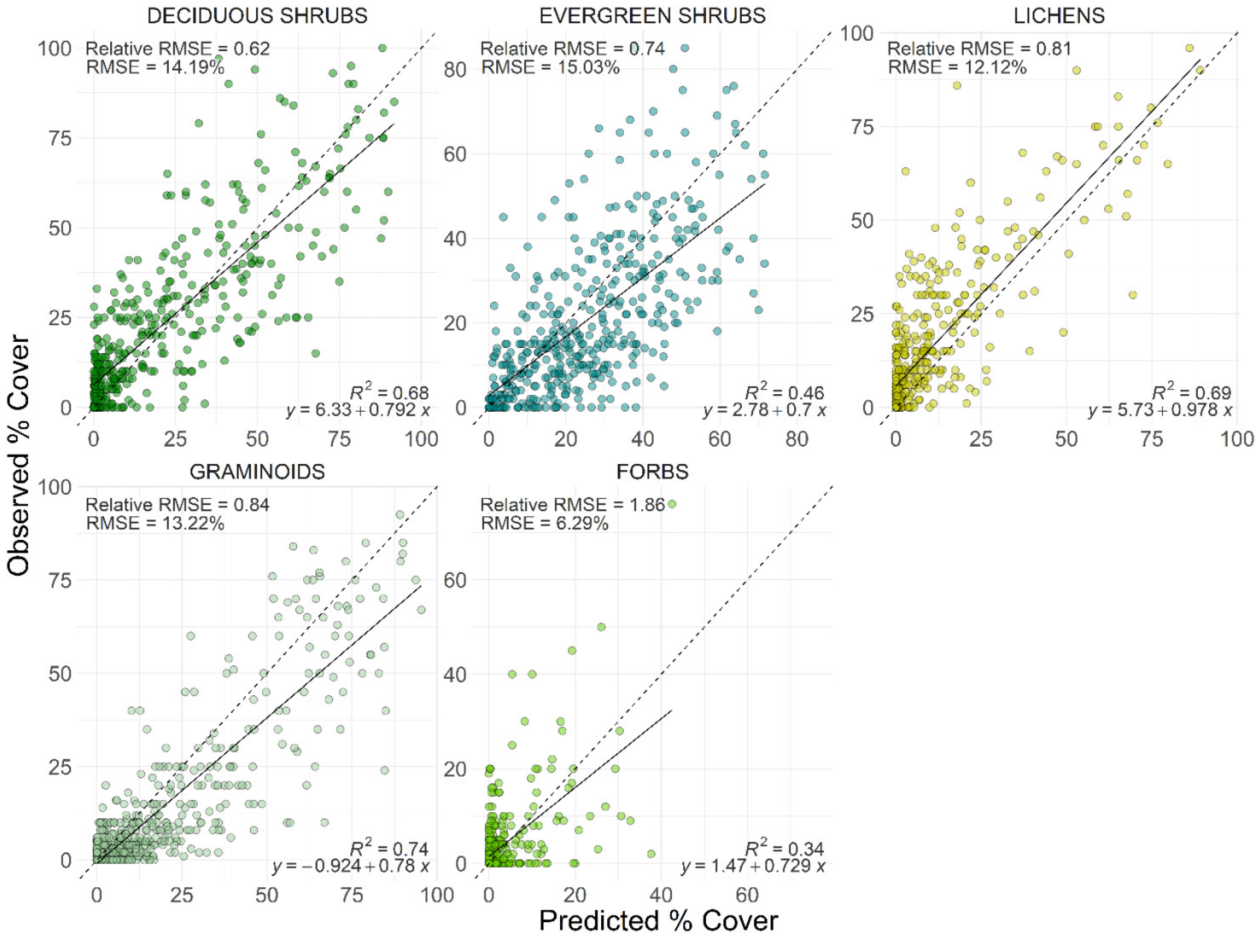

likely due to its ability to quantify vegetation greenness. PFTs were classified with an overall accuracy of 74.7% (SD = 14.2%). Among target PFTs, deciduous shrubs were classified most accurately (F1 score = 0.624) and forbs least accurately (F1 score = 0.132; Table S5).

To compare classifications to field estimates of cover, we calculated the relative root-mean-square error (rRMSE) as the RMSE between predicted and observed cover % within each quadrat, divided by the average field estimated cover for each PFT (Zolkos et al. 2013). This allowed us to compare error among PFTs systematically. Using rRMSE, the error was lowest for deciduous and evergreen shrubs and highest for forbs (Fig. 4). R^2 values were highest for deciduous shrubs, lichens, and graminoids, and best fit line slopes were close to one for all PFTs (Fig. 4).

Using the presence/absence data, we assessed the proportion of omission and commission errors across PFTs. Omission errors were most prevalent among lichens and forbs (Fig. S1, left), whereas commission errors were least prevalent among lichens (Fig. S1, right). Using the presence-only data, we compared the relative % difference across PFTs and found lichens and forbs had higher relative error than deciduous and evergreen shrubs (α = 0.05; Fig. S2).

Canopy height models

Ground/canopy segmentation of point clouds was visibly improved (Fig. S3) using PFT classification to filter point clouds. This additional filtering step produced a reasonable CHM in areas with complex terrain, like the polygonized ground shown in Fig. S4.

When we compared CHM estimates to field measured height (averaged per quadrat), we found rRMSE was lowest for deciduous shrubs and graminoids and highest for lichens and forbs (Fig. S5). Height was underestimated in the CHM in general and particularly for graminoids (Fig. S5).

Aboveground biomass

The aboveground biomass-volume linear mixed-effect model relationship was strongest for deciduous shrubs and graminoids (R^2 = 0.78, 0.75; Fig. S6) and weakest for lichens and forbs (R^2 = 0.28, 0.35; Fig. S6). When predicted biomass values (summed per quadrat) were compared to field harvested biomass, RMSE for total biomass was 220.5 g m^{-2} (extrapolated from g 0.25 m^{-2}). Among PFTs, rRMSE was lowest for deciduous and evergreen shrubs and highest for graminoids and forbs (Fig. 5). For graminoids, both rRMSE and R^2 were heavily influenced by a single poorly predicted data point. Using the presence-only data, lichens had higher

Fig. 5. Comparison of field observed biomass and predicted biomass (from linear modeling). Each point represents a quadrat. The dashed line shows the one-to-one line. The solid black line shows the line of best fit.

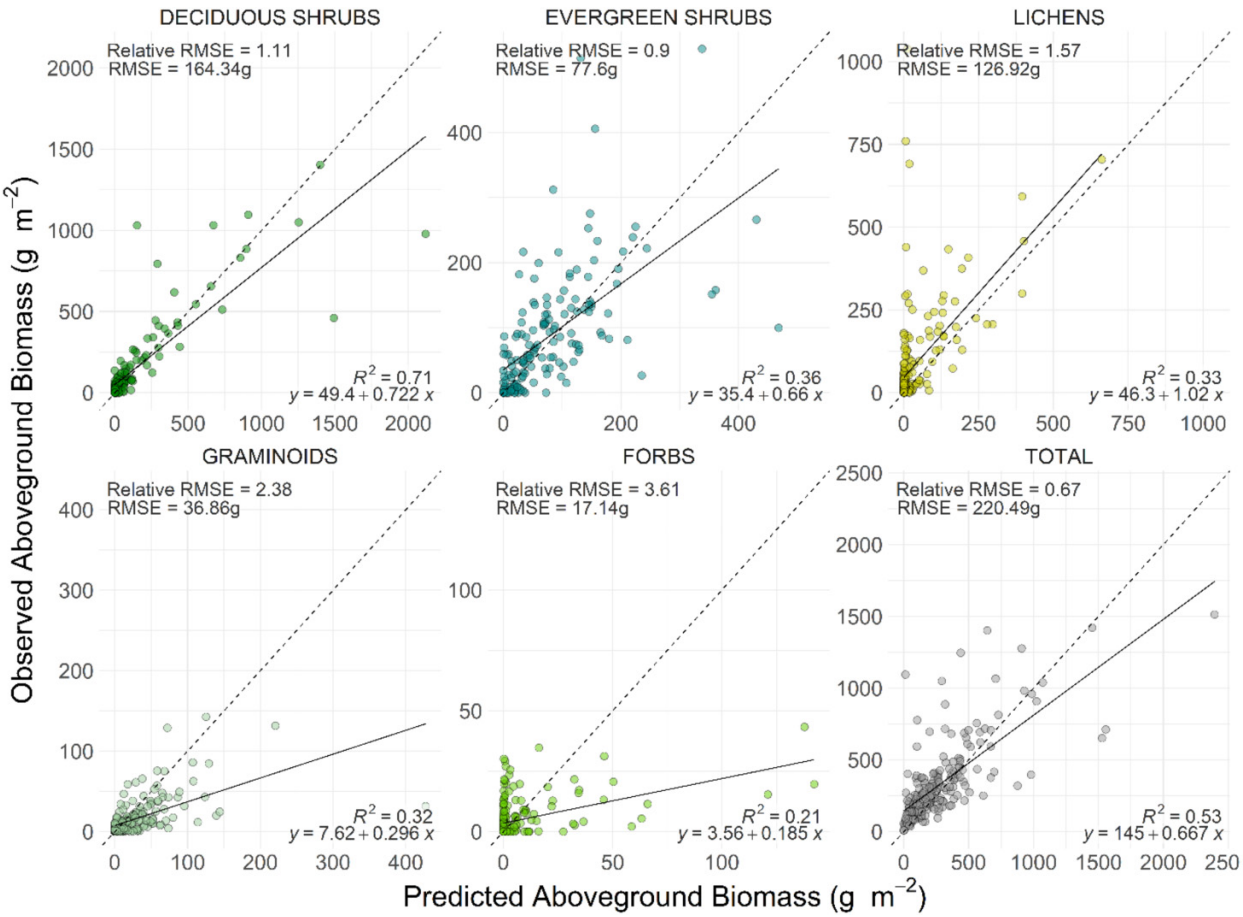

relative biomass prediction error than all other PFTs, except forbs ($\alpha = 0.05$; Fig. S7).

Comparison among vegetation community types

Differences in cover prediction error among vegetation community types alone were not statistically significant (Fig. S8). The biomass prediction error was lowest in closed low scrub, although the differences were not statistically significant (Fig. S9). Grouped by PFT, deciduous shrub cover was best predicted in open low scrub and closed tall and low scrub communities, lichen cover was best predicted in lichen-dominated communities, and graminoid cover was best predicted in mesic graminoid herbaceous communities. However, most pairwise differences between vegetation community types were not statistically significant (Fig. 6). We found similar patterns when comparing the relative % difference in biomass across PFTs and vegetation community types (Fig. S10).

Discussion

There is growing interest in using UAVs to estimate biomass of short stature vegetation owing to the large extent of such ecosystems and the many ways vegetation influences ecosystem processes and function. Research by Cunliffe et al. (2021) demonstrates that UAV-based estimates of canopy height can be used to estimate biomass across a range of PFTs in a sample of 36 sites from non-forested ecosystems around the globe. Here, we focus more intensively on 44 sites in tundra ecosystems and at the tundra/taiga ecotone. To our knowledge, ours is the first study to use UAVs to estimate aboveground biomass for a range of tundra PFTs, and the first to compare biomass predictions across a wide range of tundra vegetation communities. Our results demonstrate UAV-based structural metrics are able to accurately predict biomass across most PFTs in these biomes, illustrating the promise of using UAVs to improve our understanding of the ecology and conservation of Arctic vegetation communities. Here we discuss the challenges and achievements of our PFT UAV-based biomass estimation approach and the implications of our results for related UAV-based research.

Plant functional type classification

Our overall classification accuracy (75%) was similar to the classification by Thomson et al. (2021) (72%) but lower than the classification by Fraser et al. (2016) (82%), Yang et al. (2020) (81%), and Yang et al. (2021) (93%–95%). We believe our slightly lower accuracy (as compared to the latter studies) is due in part to the larger number of sites we classified. Here we de-

Fig. 6. Variation in relative % difference in cover estimation among vegetation community types, grouped by plant functional type. Brackets show a significance level for pairwise comparisons and are only shown for pairings with significant differences (∗: $\alpha \leq 0.05$, ∗∗: $\alpha \leq 0.01$, ∗∗∗: $\alpha \leq 0.001$, ∗∗∗∗: $\alpha \leq 0.0001$). Numbers at the bottom of the plot show the number of quadrats for each group, and boxplots are shaded to represent the average % cover among all quadrats for each group. Groups with a number of quadrats ≤2 were omitted for clarity.

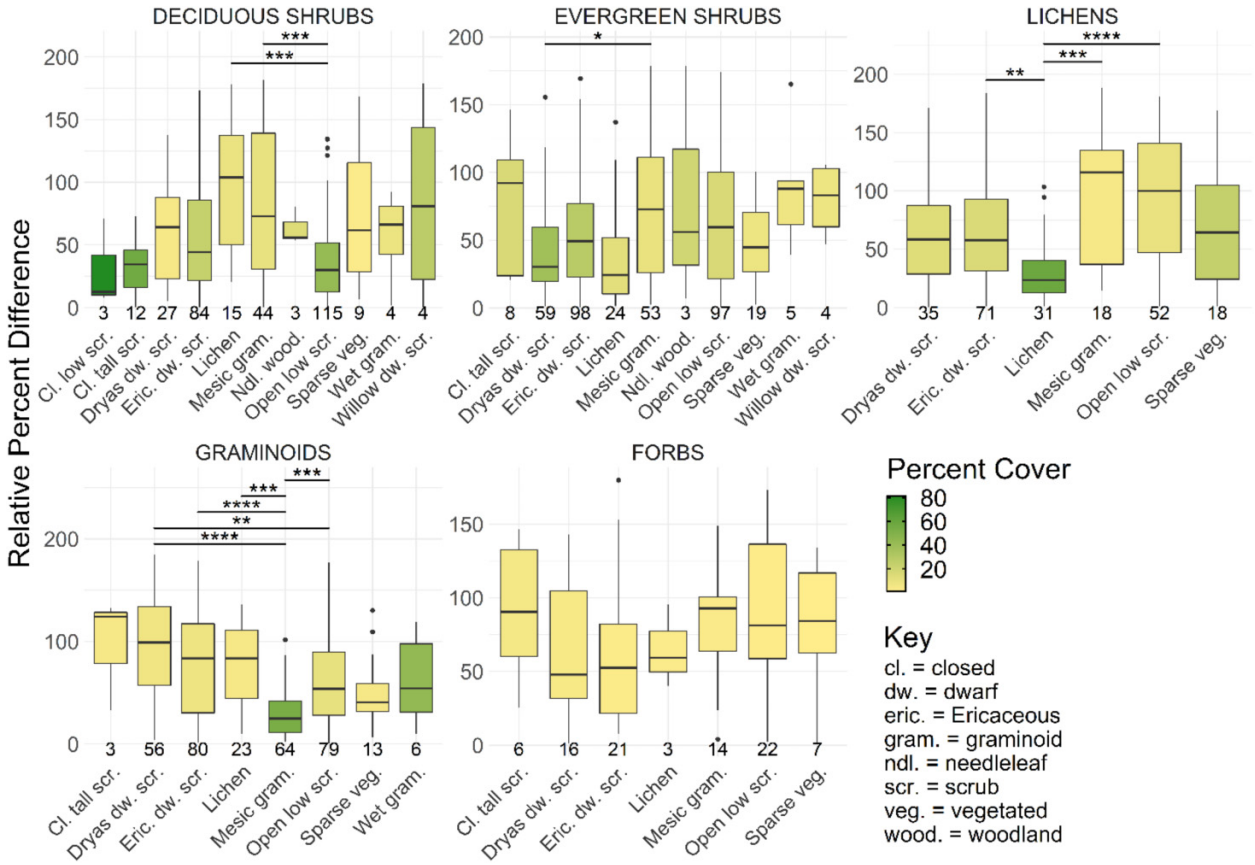

veloped a classification methodology that could be readily applied to a large number of sites ($n = 44$). In contrast, most previous UAV-based PFT mapping has been applied to only one or a few sites. Thus, the classification models can be carefully tuned to those particular sites, resulting in higher accuracy. Although the fact that our methodology was applied across a large range of sites might have resulted in slightly reduced accuracy, we believe the ability to produce a larger quantity of data across multiple landscape types was useful for our analysis and will be useful in future UAV-based research.

Among PFTs, cover of deciduous shrubs, evergreen shrubs, lichens, and graminoids was predicted best, with best-fit slopes closer to one, higher R^2 and lower rRMSE values (Fig. 4). Predicting at 30 m resolution in a similar Arctic system, Macander et al. (2017) also found shrub PFTs were predicted best, likely because shrubs typically occur in the canopy as opposed to subcanopy or ground cover. However, they reported poor performance predicting graminoids, which highlights potential challenges in scaling graminoid predictions to coarser resolution imagery (e.g., from aircraft to satellites). UAV-based graminoid classification in Arctic ecosystems has had mixed results. Graminoids were predicted best among PFTs by Yang et al. (2020), but worst among PFTs by Fraser et al. (2016). This discrepancy was likely due to differences in classification schemes. Yang et al. (2020) classified by PFT and therefore graminoids were easily distinguished from shrubs. In contrast, Fraser et al. (2016) classified by vegetation community type and thus sedge tussock and wet graminoid communities were easily confused with mixed dwarf shrub communities, which also contained sedges. Our results and those of Yang et al. (2020), however, demonstrate that when graminoids are classified discretely; they can be readily discriminated from other PFTs. UAV-based models by Macander et al. (2018) classified lichens with similar error (RMSE = 13.9%, $R^2 = 0.71$) to ours (RMSE = 12.1%, $R^2 = 0.69$) when compared to independent field-based validation data. These results show that lichens can be consistently classified with reasonable accuracy, although they tend to be slightly underpredicted. Our models also underpredicted forb cover (Fig. 4). This was likely due to forbs occurring in small groupings that are unresolved in the UAV imagery or occurring in the understory where they were obscured by canopy or shadows. Additionally, horsetails and graminoids were nearly indistinguishable in the UAV imagery and we suspect many horsetails (a forb) were incorrectly classified as graminoids. Grouping forbs and graminoids into a combined

"herbaceous" class might improve classification accuracy, as was the case for Macander et al. (2017), predicting at 30 m resolution. Our results indicate that most PFTs, with the exception of forbs, can be classified accurately across entire sites.

We built a separate classification model for each site due to differences in illumination conditions across sites. This has the drawback of making these models non-transferable to other sites or time periods. The multispectral imagery can be reflectance calibrated in Pix4Dmapper (Pix4D SA 2021) using light sensors and reflectance panels, but methods for calibrating the RGB imagery are not as well established. The RGB imagery was an important predictor in our classification, likely because it was very high resolution. Future studies might consider evaluating the transferability of classification models built from calibrated multispectral imagery as model transferability might be worth sacrificing some degree of model accuracy. We suggest the development of transferable models as a priority for future research and believe this effort will be bolstered by improving multispectral sensor technology (e.g., increases in resolution, decreases in sensor weight), and efforts to standardize UAV protocols, such as the High-Latitude Drone Ecology Network (HiLDEN, https://arcticdrones.org/). Nonetheless, standardization across sites remains a challenging issue as illumination conditions can change quickly, even within a single flight.

Canopy height models

Vegetation height is an important structural trait that is influenced by climate warming and is closely tied to competitive ability, soil properties, and carbon cycling (Bjorkman et al. 2018). Our approach to CHM creation led to underestimation of canopy height when compared to field data (Fig. S5), which is consistent with most (Chen et al. 2012; Dandois et al. 2015; Grüner et al. 2019; Wijesingha et al. 2019; Zhang et al. 2018), but not all (Cunliffe et al. 2020; Fraser et al. 2016) studies in natural systems. We suspect this was driven by the inclusion of "ground" points that were not strictly ground (e.g., moss hummocks). However, it is worth noting that field measurements might not capture the full range of variability in canopy height across an area acquired with UAV imagery (Poley and McDermid 2020).

For many of our sites, the ground surface was a complex mosaic of bryophytes, lichens, bare ground, and prostrate vascular plants. This led to complications separating the ground and canopy surfaces (Greaves et al. 2016). Most UAV studies segment the ground/canopy by identifying the lowest/highest points (e.g., progressive morphological filter), which typically results in height underestimation (Poley and McDermid 2020). Yang et al. (2020) used PFT classification results to segment the ground and canopy but also reported underestimations in the CHM. Although our CHMs underestimated vegetation height as well, we found ground/canopy segmentation using a combined approach (focal min/max and PFT classification) performed better than either approach alone. This could be a viable approach for other systems with low stature vegetation and complex topography. One drawback of this approach was an increase in processing artifacts in the CHM. This approach thus has trade-offs that need to be carefully considered in the context of mapping objectives.

Ultimately, the goal of point cloud segmentation is to produce an accurate model of the ground surface (DTM). Ground/canopy segmentation can be improved by collecting leaf-off imagery to obtain better ground views (Poley and McDermid 2020). DTMs can also be sourced elsewhere, e.g., from lidar data (Poley and McDermid 2020), or created by collecting high accuracy global navigation satellite system (GNSS) observations and interpolating between them (Cunliffe et al. 2021; Poley and McDermid 2020). However, these approaches may require additional equipment and (or) effort in the field and may be limited by availability in the case of lidar data. Externally sourced DTMs might also cause complex alignment issues in three-dimensional space (Alonzo et al. 2020).

Aboveground biomass

Aboveground biomass is another critical Arctic vegetation trait related to shrub expansion, disturbance regimes, and wildlife forage patterns (Epstein et al. 2013) and is also a major component of aboveground tundra carbon stores (Schuur et al. 2018). Our deciduous shrub RMSE of 164.3 g m^{-2} (Fig. 5) was similar to a study estimating shrub aboveground biomass from terrestrial lidar (RMSE = 108–177 g m^{-2}) (Greaves et al. 2015), and outperformed studies estimating shrub aboveground biomass from airborne lidar (RMSE = 219 g m^{-2}) (Greaves et al. 2016) and tall deciduous shrub aboveground biomass from airborne SfM (RMSE = 1260 g m^{-2}) and UAV SfM (RMSE = 810 g m^{-2}) (Alonzo et al. 2020). It is worth noting, however, that the average deciduous shrub aboveground biomass was also higher in those studies. Our deciduous shrub R^2 of 0.71 was on par with the aforementioned studies (terrestrial lidar: 0.77–0.96 (Greaves et al. 2015), airborne SfM: 0.75 (Alonzo et al. 2020), and UAV SfM: 0.82 (Alonzo et al. 2020)).

We were unable to contextualize biomass RMSE for other PFTs due to limited existing research, but our modeling results were consistent with a global study estimating the biomass of low-stature vegetation from canopy heights (Cunliffe et al. 2021). However, Cunliffe et al. (2021) reported higher R^2 values for graminoids (0.75 vs. 0.32) and forbs (0.47 vs. 0.21). We suspect the discrepancy in graminoid R^2 can be partially attributed to classification errors. Misclassified graminoid pixels might be associated with erroneously high (actually deciduous shrub) or low (actually lichen) canopy height values. Forbs were subject to classification error as well, but also suffered from being a rare and diverse PFT across tundra ecosystems. Forb data were limited and not well constrained since growth forms and spectral signatures varied considerably among species. Classification was not part of the methodology of Cunliffe et al. (2021) and thus their results were not subject to this source of error. However, classification was important in our case because it allowed us to predict PFT biomass across the entire UAV orthophoto mosaic rather than just at discrete plot locations within the mosaic.

A major difficulty in analyzing biomass predictions was identifying and quantifying sources of error (Alonzo et al.

2020; Cunliffe et al. 2020, 2021; Poley and McDermid 2020). Error in our biomass estimation was derived from multiple sources: classification error, CHM error, uncertainty in the biomass-volume relationship, error in field data used for comparison, and errors in alignment between imagery and field data. It was not possible to isolate errors from these sources, but we were able to discern several key sources of error. First, shorter stature PFTs (lichens, forbs) had higher CHM error because they were more difficult to distinguish from the ground surface. Second, PFTs with more diverse growth forms (evergreen shrubs, forbs) had greater uncertainty in their biomass-volume relationships. Finally, PFT classification error had downstream effects on height and biomass error. This highlights the difficulty of estimating biomass beyond a single PFT. However, PFT-specific biomass mapping adds ecologically relevant details that are not widely available from satellite image-based mapping and is thus a worthwhile endeavor (Berner et al. 2018; Chen et al. 2012). For example, our results indicate that UAV-based methods may be able to track the consequences of Arctic vegetation change such as shrub expansion on graminoid, forb, and lichen functional traits (cover, height, biomass, etc.). Tracking such vegetation changes also has conservation applications such as monitoring wildlife forage (e.g., lichen as a critical food source for many at-risk Arctic caribou populations) and understanding how disturbance alters patterns of vegetation distribution.

Comparison among vegetation community types

When grouped by PFT, cover and biomass prediction error were lowest in communities where the PFT of interest was abundant and dominant (Figs. 6 and S10). In their Landsat-based mapping of lichen cover, Macander et al. (2020) and Kennedy et al. (2020) similarly noted that lichens were predicted worst at low abundances. Though not statistically significant, there was some evidence that graminoid cover and biomass predictions were better in mesic graminoid herbaceous communities (i.e., tussock tundra) than in other communities with equally high graminoid abundance (wet graminoid herbaceous; Figs. 6 and S10). Mapping at 30 m resolution, Nawrocki et al. (2020) similarly found tussock-forming sedges were predicted better than non-tussock forming sedges, even though they were equally abundant. However, UAV-based mapping by Fraser et al. (2016) found the opposite—non-tussock tundra was predicted slightly better than tussock tundra.

Overall our results echo previous studies: PFTs were classified better in communities where they were part of the canopy, more distinct, and (or) more abundant. However, our results also highlight the promise of UAV-based cover and biomass estimation in tussock tundra communities, which have not been well predicted in the past (Fraser et al. 2016; Macander et al. 2017).

Conclusion

Our results add to a growing body of work suggesting that low-cost UAV platforms can be leveraged to estimate the aboveground biomass of vegetation in tundra landscapes with reasonably high accuracy (Alonzo et al. 2020; Cunliffe et al. 2020, 2021; Poley and McDermid 2020; Yang et al. 2020). The RMSE values we report for deciduous shrub biomass estimates are comparable to previous studies (Alonzo et al. 2020; Greaves et al. 2015, 2016), but we also went beyond deciduous shrubs to provide some of the first UAV-based biomass predictions for other Arctic PFTs, with all results validated by field harvest data. The biomass prediction results for graminoids in tussock tundra, and evergreen shrubs were encouraging, but we were unable to robustly compare our prediction accuracy to other studies due to a lack of existing UAV-based estimates of biomass. Lichens were less well predicted, but again few UAV-based estimates of biomass exist for comparison. This may change in the future with the advancement of HiLDEN (High-Latitude Drone Ecology Network, 2021).

Biomass estimation of tundra PFTs is a valuable area for future research, particularly in the context of rapid advancements in UAV mapping and application to ecological problems. As the Arctic landscape continues to change, monitoring all PFTs, not just tall shrubs, will be crucial in making informed decisions regarding climate policy, land, and wildlife management. Our results suggest UAV-based estimates of biomass could provide a valuable step from field measurements to regional scale maps of vegetation biomass, partitioned by PFT. Such maps would allow researchers to track ecologically meaningful changes across remote Arctic landscapes, such as those driven by increases in wildfire frequency and severity, shrub expansion, and (or) human land use change.

Acknowledgements

The authors extend heartfelt thanks to Mike Suitor (Yukon Government), Dave Tavares (Parks Canada), and Joe Costa (Parks Canada) for logistical support throughout the project. For their support of our research, the authors extend thanks to Yukon-Charley Rivers National Park (YUCH-2018SCI-0004), Yukon Government (19–64S&E), Ivvavik National Park (IVV-2019–32638), the Wildlife Management Advisory Council—North Slope, the Tetlin Renewable Resource Council, the Gwich'in Renewable Resources Board, and the Aklavik Hunters and Trappers Committee. Unmanned aerial vehicle (UAV) operation was conducted by FAA-certified SUAS operators and was permitted in Canada under a Special Flight Operations Certificate (920010). Field work was a collaborative effort supported by Craig Townsend, Joël Potié, Elis Juhlin, Abby Rutrough, Aerin Jacob, Kayla Arey, Laurence Carter, Martin Kienzler, Sonny Parker, Hayleigh Conway, and Andrew Davies. The authors thank them for their assistance in collecting high-quality data that made this research possible. Additional thanks are extended to Gabrielle Coulombe and Andrew Davies for help in the laborious task of processing field biomass harvest data, to Gabrielle Coulombe for assistance with data entry, to Matt Macander and Eric Palm for expert advice on UAV operations and processing, and to Patrick Burns, Logan Berner, Chris Doughty, and Michelle Mack for

providing valuable feedback on various aspects of the research approach.

Article information

History dates

Received: 30 August 2021
Accepted: 8 March 2022
Accepted manuscript online: 12 April 2022
Version of record online: 18 August 2022

Notes

This paper is part of a Collection on Unoccupied Vehicle Systems in Arctic Research and Monitoring jointly published by *Arctic Science* and *Drone Systems and Applications*.

Copyright

Data availability

Data supporting the results in this paper are publicly archived at the National Science Foundation Arctic Data Center: https://doi.org/10.18739/A2R785Q5B.

Author information

Author ORCIDs

Kathleen M. Orndahl https://orcid.org/0000-0002-4873-4375

Author contributions

KMO and SJG conceived the ideas; KMO, LPWE, and JDH designed the methodology; KMO, LPWE, JDH, and REP collected the data; KMO, LPWE, and REP processed and curated the data; KMO analyzed the data with input from MH; KMO led the writing of the manuscript. All authors contributed to writing and editing.

Competing interests

The authors declare there are no competing interests.

Funding information

This material is based upon work supported by the National Science Foundation Graduate Research Fellowship under Grant No. 1938054 (to KMO), NASA ABoVE grants NNX17AE44 G and 80NSSC19M0112 (to SJG), the Bureau of Land Management, the USDA National Institute of Food and Agriculture, McIntire Stennis project 1021603 (to MH), and the Navigating the New Arctic NSF grant #2127272 (to MH).

Supplementary material

Supplementary data are available with the article at https://doi.org/10.1139/AS-2021-0044.

References

Abbott, B.W., Jones, J.B., Schuur, E.A.G., Chapin, F.S., Bowden, W.B., Bret-Harte, M.S., et al. 2016. Biomass offsets little or none of permafrost carbon release from soils, streams, and wildfire: an expert assessment. Environmental Research Letters, **11**: 034014. doi:10.1088/1748-9326/11/3/034014.

Alonzo, M., Dial, R.J., Schulz, B.K., Andersen, H.-E., Lewis-Clark, E., and Cook, B.D., 2020. Mapping tall shrub biomass in Alaska at landscape scale using structure-from-motion photogrammetry and lidar. Remote Sensing of Environment, **245**: 111841. doi:10.1016/j.rse.2020.111841.

Assmann, J.J., Kerby, J.T., Cunliffe, A.M., and Myers-Smith, I.H. 2019. Vegetation monitoring using multispectral sensors—best practices and lessons learned from high latitudes. Journal of Unmanned Vehicle Systems, **7**: 54–75. doi:10.1139/juvs-2018-0018.

Bates, D., Mächler, M., Zurich, E., Bolker, B.M., and Walker, S.C. 2014. Fitting linear mixed-effects models using lme4. arXiv:1406.5823.

Berner, L.T., Jantz, P., Tape, K.D., and Goetz, S.J. 2018. Tundra plant aboveground biomass and shrub dominance mapped across the north slope of Alaska. Environmental Research Letters, **13**: 035002. doi:10.1088/1748-9326/aaaa9a.

Berner, L.T., Massey, R., Jantz, P., Forbes, B.C., Macias-Fauria, M., Myers-Smith, I., et al. 2020. Summer warming explains widespread but not uniform greening in the arctic tundra biome. Nature Communication, **11**: 4621. doi:10.1038/s41467-020-18479-5.

Bernes, C., Bråthen, K.A., Forbes, B.C., Speed, J.D.M., and Moen, J. 2015. What are the impacts of reindeer/caribou (*Rangifer tarandus* L.) on arctic and alpine vegetation? A systematic review. Environmental Evidence, **4**: 4. doi:10.1186/s13750-014-0030-3.

Bjorkman, A.D., García Criado, M., Myers-Smith, I.H., Ravolainen, V., Jónsdóttir, I.S., Westergaard, K.B., et al. 2020. Status and trends in arctic vegetation: evidence from experimental warming and long-term monitoring. Ambio, **49**: 678–692. doi:10.1007/s13280-019-01161-6. PMID: 30929249.

Bjorkman, A.D., Myers-Smith, I.H., Elmendorf, S.C., Normand, S., Rüger, N., Beck, P.S.A., et al.. 2018. Plant functional trait change across a warming tundra biome. Nature. **562**: 57–62. doi:10.1038/s41586-018-0563-7. PMID: 30258229.

Bolker, B.M. 2021. GLMM FAQ [WWW Document]. Available from https://bbolker.github.io/mixedmodels-misc/glmmFAQ.html[accessed 7 June 2021].

Chapin, F.S. 2003. Effects of plant traits on ecosystem and regional processes: a conceptual framework for predicting the consequences of global change. Annals of Botany, **91**: 455–463. doi:10.1093/aob/mcg041. PMID: 12588725.

Chapin, F.S., Bret-Harte, M.S., Hobbie, S.E., and Zhong, H. 1996. Plant functional types as predictors of transient responses of arctic vegetation to global change. Journal of Vegetation Science, **7**: 347–358. doi:10.2307/3236278.

Chapin, F.S., Sturm, M., Serreze, M.C., McFadden, J.P., Key, J.R., Lloyd, A.H., et al.. 2005. Role of land-surface changes in arctic summer warming. Science, **310**: 657–660. doi:10.1126/science.1117368.

Chen, W., Chen, W., Li, J., Zhang, Y., Fraser, R., Olthof, I., et al.. 2012. Mapping aboveground and foliage biomass over the porcupine Caribou habitat in northern Yukon and Alaska using Landsat and JERS-1/SAR data. *In* Remote sensing of biomass - principles and applications. *Edited by* T. Fatoyinbo. InTech, Rijeka, Croatia, pp. 231–252. doi:10.5772/19219.

CloudCompare. 2021. (version 2.11.3) [GPL software]. Available from http://www.cloudcompare.org/.

Cunliffe, A.M., Anderson, K., Boschetti, F., Brazier, R.E., Graham, H.A., Myers-Smith, I.H., et al.. 2021. Global application of an unoccupied aerial vehicle photogrammetry protocol for predicting aboveground biomass in non-forest ecosystems. Remote Sensing in Ecology and Conservation. doi:10.1002/RSE2.228. PMID: 33889421.

Cunliffe, A.M., Brazier, R.E., and Anderson, K. 2016. Ultra-fine grain landscape-scale quantification of dryland vegetation structure with drone-acquired structure-from-motion photogrammetry. Remote Sensing of Environment, **183**: 129–143. doi:10.1016/j.rse.2016.05.019.

Cunliffe, A.M., Assmann, J.J., Daskalova, G.N., Kerby, J.T., and Myers-Smith, I.H. 2020. Aboveground biomass corresponds strongly with

drone-derived canopy height but weakly with greenness (NDVI) in a shrub tundra landscape. Environmental Research Letters, **15**: 125004. doi:10.1088/1748-9326/aba470.

Dandois, J.P., Olano, M., and Ellis, E.C. 2015. Optimal altitude, overlap, and weather conditions for computer vision UAV estimates of forest structure. Remote Sensing, **7**: 13895–13920. doi:10.3390/rs71013895.

Environmental Systems Research Institute Inc. 2021. ArcGIS Pro. (version 2.7.1). Redlands, CA, Available from https://www.esri.com/en-us/arcgis/products/arcgis-pro/overview.

Epstein, H.E., Myers-Smith, I., and Walker, D.A. 2013. Recent dynamics of arctic and sub-arctic vegetation. Environmental Research Letters, **8**: 015040. doi:10.1088/1748-9326/8/1/015040.

Fletcher, D., MacKenzie, D., and Villouta, E. 2005. Modelling skewed data with many zeros: a simple approach combining ordinary and logistic regression. Environmental and Ecological Statistics, **12**: 45–54. doi:10.1007/s10651-005-6817-1.

Fraser, R.H., Olthof, I., Lantz, T.C., and Schmitt, C. 2016. UAV photogrammetry for mapping vegetation in the low-Arctic. Arctic Science, **2**: 79–102. doi:10.1139/as-2016-0008.

Greaves, H.E., Vierling, L.A., Eitel, J.U.H., Boelman, N.T., Magney, T.S., and Prager, C.M., 2016. High-resolution mapping of aboveground shrub biomass in arctic tundra using airborne lidar and imagery. Remote Sensing of Environment, **184**: 361–373. doi:10.1016/j.rse.2016.07.026.

Greaves, H.E., Vierling, L.A., Eitel, J.U.H., Boelman, N.T., Magney, T.S., and Prager, C.M., 2015. Estimating aboveground biomass and leaf area of low-stature arctic shrubs with terrestrial LiDAR. Remote Sensing of Environment, **164**: 26–35. doi:10.1016/j.rse.2015.02.023.

Grüner, E., Astor, T., and Wachendorf, M. 2019. Biomass prediction of heterogeneous temperate grasslands using an SfM approach based on UAV Imaging. Agronomy, **9**: 54. doi:10.3390/agronomy9020054.

High-Latitude Drone Ecology Network 2021. Drone Ecology Network – Using drones to study high-latitude ecology [WWW Document]. Available from https://arcticdrones.org/ [accessed 7 August 21].

Houghton, R.A., Hall, F., and Goetz, S.J. 2009. Importance of biomass in the global carbon cycle. Journal of Geophysics Research Biogeosciences, **114**, 1–13. doi:10.1029/2009JG000935.

Huang, B.F.F., and Boutros, P.C. 2016. The parameter sensitivity of random forests. BMC Bioinformatics, **17**: 331. doi:10.1186/s12859-016-1228-x. PMID: 27586051.

Kennedy, B., Pouliot, D., Manseau, M., Fraser, R., Duffe, J., Pasher, J., et al. 2020. Assessment of Landsat-based terricolous macrolichen cover retrieval and change analysis over Caribou ranges in northern Canada and Alaska. Remote Sensing of Environment, **240**: 111694. doi:10.1016/j.rse.2020.111694.

Lafleur, P.M., and Humphreys, E.R. 2018. Tundra shrub effects on growing season energy and carbon dioxide exchange. Environmental Research Letters, **13**: 055001. doi:10.1088/1748-9326/aab863.

Langford, Z., Kumar, J., Hoffman, F.M., Norby, R.J., Wullschleger, S.D., and Sloan, V.L., 2016. Mapping arctic plant functional type distributions in the barrow environmental observatory using worldview-2 and LiDAR datasets. Remote Sensing, **8**: 733. doi:10.3390/RS8090733.

Lawrence, D.M., and Swenson, S.C. 2011. Permafrost response to increasing arctic shrub abundance depends on the relative influence of shrubs on local soil cooling versus large-scale climate warming. Environmental Research Letters, **6**: 045504. doi: 10.1088/1748-9326/6/4/045504.

Lemaître, G., Nogueira, F., and Aridas, C.K. 2017. Imbalanced-learn: a python toolbox to tackle the curse of imbalanced datasets in machine learning. Journal of Machine Learning Research, **18**, 1–5.

Loranty, M.M., and Goetz, S.J. 2012. Shrub expansion and climate feedbacks in arctic tundra. Environmental Research Letters, **7**: 011005. doi: 10.1088/1748-9326/7/1/011005.

Lortie, C.J., Brooker, R.W., Choler, P., Kikvidze, Z., Michalet, R., and Pugnaire, F.I., 2004. Rethinking plant community theory. Oikos, **107**: 433–438. doi:10.1111/J.0030-1299.2004.13250.X.

Lundberg, S.M., Erion, G., Chen, H., DeGrave, A., Prutkin, J.M., Nair, B., et al. 2020. From local explanations to global understanding with explainable AI for trees. Nature Machine Intelligence, **2**: 56–67. doi:10.1038/s42256-019-0138-9. PMID: 32607472.

Macander, M.J., Frost, G.V., and Palm, E.C. 2018. Lichen cover mapping for the range of the Fortymile caribou herd, Alaska and Yukon Territory. Prepared for Bureau of Land Management and Department of Environment Government of Yukon.

Macander, M.J., Frost, G.V., Nelson, P.R., and Swingley, C.S. 2017. Regional quantitative cover mapping of tundra plant functional types in Arctic Alaska. Remote Sensing, **9**, 1–26. doi:10.3390/rs9101024.

Macander, M.J., Palm, E.C., Frost, G.V, Herriges, J.D., Nelson, P.R., Roland, C., et al. 2020. Lichen cover mapping for caribou ranges in interior Alaska and Yukon. Environmental Research Letters, **15**: 55001. doi:10.1088/1748-9326/ab6d38.

Mack, M.C., Schuur, E.A.G., Bret-Harte, M.S., Shaver, G.R., and Chapin, F.S. 2004. Ecosystem carbon storage in arctic tundra reduce by long-term nutrient fertilization. Nature, **431**: 440–443. doi:10.1038/nature02887. PMID: 15386009.

Mallory, C.D., and Boyce, M.S. 2018. Observed and predicted effects of climate change on Arctic Caribou and reindeer. Environmental Review, **26**: 13–25. doi:10.1139/er-2017-0032.

Morrison, L.W. 2016. Observer error in vegetation surveys: a review. Journal of Plant Ecology, **9**: 367–379. doi:10.1093/JPE/RTV077.

Myers-Smith, I.H., Grabowski, M.M., Thomas, H.J.D., Angers-Blondin, S., Daskalova, G.N., Bjorkman, A.D., et al. 2019. Eighteen years of ecological monitoring reveals multiple lines of evidence for tundra vegetation change. Ecological Monographs, **89**: e01351. doi:10.1002/ecm.1351.

Myers-Smith, I.H., Kerby, J.T., Phoenix, G.K., Bjerke, J.W., Epstein, H.E., Assmann, J.J., et al. 2020. Complexity revealed in the greening of the Arctic. Nature Climate Change, **10**: 106–117. doi:10.1038/s41558-019-0688-1.

Nandlall, S.D., and Millard, K. 2020. Quantifying the relative importance of variables and groups of variables in remote sensing classifiers using Shapley values and game theory. IEEE Geoscience and Remote Sensing Letters, **17**: 42–46. doi:10.1109/LGRS.2019.2914374.

Nauta, A.L., Heijmans, M.M.P.D., Blok, D., Limpens, J., Elberling, B., Gallagher, A., et al. 2015. Permafrost collapse after shrub removal shifts tundra ecosystem to a methane source. Nature Climate Change, **5**: 67–70. doi:10.1038/nclimate2446.

Nawrocki, T.W., Carlson, M.L., Osnas, J.L.D., Trammell, E.J., and Witmer, F.D.W. 2020. Regional mapping of species-level continuous foliar cover: beyond categorical vegetation mapping. Ecological Applications, **30**: e02081. doi:10.1002/EAP.2081. PMID: 31971646.

Olofsson, J., and Post, E. 2018. Effects of large herbivores on tundra vegetation in a changing climate, and implications for rewilding. Philosophical Transactions of the Royal Society B: Biological Sciences, **373**: 20170437. doi:10.1098/rstb.2017.0437.

Pearson, R.G., Phillips, S.J., Loranty, M.M., Beck, P.S.A., Damoulas, T., and Knight, S.J., 2013. Shifts in arctic vegetation and associated feedbacks under climate change. Nature Climate Change, **3**: 673–677. doi:10.1038/nclimate1858.

Pedregosa, F., Varoquaux, G., Gramfort, A., Michel, V., Thirion, B., Grisel, O., et al. 2011. Scikit-learn: machine learning in Python. Journal of Machine Learning Research, **12**: 2825–2830.

Pix4D SA 2021. Pix4Dmapper. Prilly, Switzerland, Available from https://www.pix4d.com/.

Poley, L.G., and McDermid, G.J. 2020. A systematic review of the factors influencing the estimation of vegetation aboveground biomass using unmanned aerial systems. Remote Sensing, **12**: 1052. doi:10.3390/rs12071052.

Post, E., Christensen, T.R., Elberling, B., Fox, A.D., Gilg, O., Stirling, I., et al. 2009. Ecological dynamics across the Arctic associated with recent climate change. Science, **325**: 1355–1258. doi:10.1126/science.1173113.

Probst, P., Wright, M.N., and Boulesteix, A. 2019. Hyperparameters and tuning strategies for random forest. Wiley Interdisciplinary Reviews: Data Mining and Knowledge Discovery, **9**: e1301. doi:10.1002/widm.1301.

R Core Team 2020. R: A language and environment for statistical computing. Vienna, Austria. Available from https://www.r-project.org/.

Räsänen, A., Juutinen, S., Aurela, M., and Virtanen, T. 2018. Predicting aboveground biomass in arctic landscapes using very high spatial resolution satellite imagery and field sampling. International Journal of Remote Sensing, **40**: 1175–1199. doi:10.1080/01431161.2018.1524176.

Richter-Menge, J., Druckenmiller, M.L., and Jeffries, M. 2019. Arctic Report 2019. NOAA.doi:10.1002/2014JC010136.

Riihimäki, H., Luoto, M., and Heiskanen, J. 2019. Estimating fractional cover of tundra vegetation at multiple scales using unmanned aerial systems and optical satellite data. Remote Sensing of Environment, **224**: 119–132. doi:10.1016/j.rse.2019.01.030.

Roussel, J.-R., and Auty, D. 2020. Airborne LiDAR Data Manipulation and Visualization for Forestry Applications. R package version 3.0.4. Available from https://cran.r-project.org/package=lidR.

Roussel, J.-R., Auty, D., Coops, N.C., Tompalski, P., Goodbody, T.R., Sanchez Meador, A., et al.. 2020. lidR: an R package for analysis of airborne laser scanning (ALS) data. Remote Sensing of Environment, **251**: 112061. doi:10.1016/j.rse.2020.112061.

Scenarios Network for Alaska and Arctic Planning 2009. Historical Derived DOF/DOT/LOGS - 2 km CRU TS. Available from http://ckan.snap.uaf.edu/ar/dataset/historical-derived-dof-dot-logs-2-km-cru-ts.

Schmitz, O.J., Wilmers, C.C., Leroux, S.J., Doughty, C.E., Atwood, T.B., Galetti, M., et al. 2018. Animals and the zoogeochemistry of the carbon cycle. Science, **362**: 1–10. doi:10.1126/science.aar3213.

Schuur, E.A.G., McGuire, A.D., Schädel, C., Grosse, G., Harden, J.W., Hayes, D.J., et al. 2015. Climate change and the permafrost carbon feedback. Nature, **520**: 171–179. doi:10.1038/nature14338. PMID: 25855454.

Schuur, E.A.G., McGuire, A.D., Schädel, C., Romanovsky, V.E., and Mack, M.C. 2018. Chapter 11: arctic and boreal carbon, *In*: Second State of the Carbon Cycle Report (SOCCR2): A Sustained Assessment Report. *Edited by* N. Cavallaro, G. Shrestha, R. Birdsey, M.A. Mayes, R.G. Najjar, S.C. Reed, et al., U.S. Global Change Research Program, Washington, DC, USA, pp. 428–468. doi:10.7930/SOCCR2.2018.Ch11.

Siewert, M.B., and Olofsson, J. 2020. Scale-dependency of arctic ecosystem properties revealed by UAV. Environmental Research Letters, **15**: 129601. doi:10.1088/1748-9326/aba20b.

Sun, Y., Wong, A.K.C., and Kamel, M.S. 2009. Classification of imbalanced data: a review. International Journal of Pattern Recognition and Artificial Intelligence, **23**: 687–719. doi:10.1142/S0218001409007326.

Thomas, H.J.D., Myers-Smith, I.H., Bjorkman, A.D., Elmendorf, S.C., Blok, D., Cornelissen, J.H.C., et al.. 2018. Traditional plant functional groups explain variation in economic but not size - related traits across the tundra biome. Global Ecology and Biogeography, **28**(2): 78–95. doi:10.1111/geb.12783.

Thomson, E.R., Spiegel, M.P., Althuizen, I.H.J., Bass, P., Chen, S., Chmurzynski, A., et al.. 2021. Multiscale mapping of plant functional groups and plant traits in the high arctic using field spectroscopy, UAV imagery and Sentinel-2A data. Environmental Research Letters, **16**: 55006. doi:10.1088/1748-9326/abf464.

Turetsky, M.R., Bond-Lamberty, B., Euskirchen, E., Talbot, J., Frolking, S., and McGuire, A.D., 2012. The resilience and functional role of moss in boreal and arctic ecosystems. New Phytology, **196**: 49–67. doi:10.1111/J.1469-8137.2012.04254.X. PMID: 22924403.

Van Rossum, G., and Drake, F.L. 2009. Python 3 Reference Manual. CreateSpace, Scotts Valley, CA.

Viereck, L.A., Dyrness, C.T., Batten, A.R., and Wenzlick, K.J. 1992. The Alaska vegetation classification., Gen. Tech. Rep. PNW-GTR-286. U.S. Department of Agriculture, Forest Service, Pacific Northwest Research Station, Portland, OR. p. 278. doi:10.2737/PNW-GTR-286.

Walker, D.A., Raynolds, M.K., Daniëls, F.J.A., Einarsson, E., Elvebakk, A., Gould, W.A., et al. 2005. The circumpolar arctic vegetation map. Journal of Vegetation Science, **16**: 267–282. doi:10.1111/j.1654-1103.2005.tb02365.x.

Wijesingha, J., Moeckel, T., Hensgen, F., and Wachendorf, M. 2019. Evaluation of 3D point cloud-based models for the prediction of grassland biomass. The International Journal of Applied Earth Observation and Geoinformation, **78**: 352–359. doi:10.1016/j.jag.2018.10.006.

Wilson, J.B. 2011. Cover plus: ways of measuring plant canopies and the terms used for them. Journal of Vegetation Science, **22**: 197–206. doi:10.1111/j.1654-1103.2010.01238.x.

Wolak, M. 2016. ICC: Facilitating Estimation of the Intraclass Correlation Coefficient. R package version 2.3.0. Available from https://cran.r-project.org/web/packages/ICC/ICC.pdf.

Yang, D., Meng, R., Morrison, B.D., McMahon, A., Hantson, W., Hayes, D.J., et al. 2020. A multi-sensor unoccupied aerial system improves characterization of vegetation composition and canopy properties in the arctic tundra. Remote Sensing, **12**: 2638. doi:10.3390/RS12162638.

Yang, D., Morrison, B.D., Hantson, W., Breen, A.L., McMahon, A., Li, Q., et al. 2021. Landscape-scale characterization of arctic tundra vegetation composition, structure, and function with a multi-sensor unoccupied aerial system. Environmental Research Letters, **16**: 085005. doi:10.1088/1748-9326/AC1291.

Zhang, H., Sun, Y., Chang, L., Qin, Yu, Chen, J., Qin, Y., et al. 2018. Estimation of grassland canopy height and aboveground biomass at the quadrat scale using unmanned aerial vehicle. Remote Sensing, **10**: 851. doi:10.3390/rs10060851.

Zolkos, S.G., Goetz, S.J., and Dubayah, R. 2013. A meta-analysis of terrestrial aboveground biomass estimation using lidar remote sensing. Remote Sensing of Environment, **128**: 289–298. doi:10.1016/j.rse.2012.10.017.